Growth of Continental Plateaus by Channel Injection: Constraints and Thermo-Mechanical Consistency

Sergei Medvedev[1,2] **and Christopher Beaumont**[1]

[1]Department of Oceanography, Dalhousie University, Halifax, NS, B3H4J1 Canada

[2]Fachrichtung Geologie, Freie Universität Berlin, Malteserstrasse 74-100, Berlin, 12249 Germany (corresponding address, e-mail: sergeim@zedat.fu-berlin.de)

Words count: 8528

References: 17

Tables: 1

Figures: 15

Abbreviated title: Growth of Plateaus by Channel Injection

Abstract

Weak, possibly partially molten, middle crust may exist and deform by channel flow beneath continental plateaus, thereby significantly influencing their dynamics. The role of channel flows in the transition zone between the plateau and the foreland is, however, unclear. We develop successively more complete approximate models for the Channel Injection (CI) mode in which differential pressure pumps channel material from beneath the plateau into the transitional crust, thickens it, and widens the plateau. The motivation is to improve our understanding of the controls on the growth of continental plateaus and the interactions in the transition zone, and to gain more insight into the results of more complex numerical models. In CI-1, a channel with constant viscosity and thickness exists in the transitional crust and the pumped material accretes/freezes above and below the channel. Although results compare favorably with the geometry of some natural examples, this model is incomplete because there is no theory for the connection to the plateau. CI-2 includes a decrease in channel viscosity when the channel depth exceeds a critical value, D^*, a proxy for onset of melt weakening or low viscosities at high temperatures. It completes the connection to the plateau but relies on the arbitrary choice of D^*. CI-3 is more physically based and considers the channel viscosity and thickness to depend on temperature, calculated by an associated thermal model that includes radioactive self-heating, and advection of heat by channel material. This model demonstrates self-consistent plateau widening if the channel viscosity decreases at the critical temperature, T^*. Acceptable comparisons with the topography of Tibet are achieved with transition zone viscosities that decrease from 10^{19}–10^{22} Pa·s to sub-plateau values of 10^{18}–10^{19} Pa·s, with T^* of 700–750°C. Additional analysis and tests are used to determine the range of parameter values for which CI models are both internally consistent and compatible with observations. Additional modes of deformation in the transition zone, Viscous Thickening (VT) and Plastic Translation (PT), may also be important. (**end of Abstract**)

High temperatures and partial melting may lead to low viscosity channel flows in the mid to lower crust beneath continental plateaus (Fig. 1a). Following earlier work demonstrating the feasibility of such channel flows (e.g., Bird 1991, Kaufman & Royden 1994), several recent studies indicate that these flows lead to decoupling of deformation with focussed flow in the channel and overlying crust that remains relatively stable (e.g., Royden 1996; Beaumont *et al.* 2001, 2004; Shen *et al.* 2001; Vanderhaeghe *et al.* 2003). These models also predict that plateaus grow outward by tectonic thickening and accretion of adjacent crust in the transition zone between the plateau and the surrounding foreland (Fig. 1c) and that channel flows may subsequently convert convert the transition zone to become part of the plateau. In contrast, Clark & Royden (2000) proposed that crust in the transition zone may thicken by direct injection of channel material (Fig. 1b) and showed this style to be compatible with the crustal thickening of the eastern margin of the Tibetan plateau. In this proposed Channel Injection (CI) mode no crustal shortening in the transition zone is required, as suggested by the limited shortening observed from the eastern margin of the Tibetan plateau.

A primary motivation for the further development of channel injection models, as described here, is to improve our understanding of the first-order controls on the growth of continental plateaus and the interactions that occur within the transition zone. The second motivation is to gain more insight into predictions of numerical models which produce realistic looking results but are difficult to interpret in terms of the basic physical controls (Beaumont *et al.* 2001, 2004; Jamieson *et al.* 2004). We investigate some of the basic factors controlling channel flows and ask whether they contribute to the outward growth of plateaus as in the channel injection mode.

The concepts that form the basis for this work (Fig. 1) rely on the exixtence of weak crust beneath plateaus. The existence of weak sub-plateau crust is also consistent with the "flat" plateau topography in that weak mid- to lower crust implies that the viscosity here is

too low to create sufficient deviatoric stress to maintain long wavelength components of the topography, and therefore plateaus flatten like pancake batter. In contrast, steep topographic gradients in the plateau-flanking transition zones (Fig. 1a) imply stronger, higher effective viscosity crust, and/or a change in boundary conditions that allows these zones to laterally support (like bookends) the plateau against its tendency to flow outward. In the limit, very weak sub-plateau crust will undergo outward channel flow driven by the pressure gradient between the plateau and the foreland (Fig. 1a), but can this limited differential pressure inject channel material into the transition zone?

Possible mechanisms for crustal thickening in the transition zone can be modelled as channel injection (Fig.1 1b, Clark & Royden 2000), viscous tectonic thickening (Fig. 1c, Royden 1996, Shen *et al.* 2001), and plastic translation (Fig. 1d, Lehner 2000, Gemmer *et al.* 2004), in which the upper brittle, frictional-plastic crust decouples and rides outward above the ductile substratum. Channel injection can thicken the transitional crust without surface shortening, but viscous thickening and plastic translation require tectonic contraction, and in the last instance extension as well.

Two end-member settings also exist for plateau growth: the "actively convergent margins" of the plateau for which contraction is imposed at the lithospheric scale by large-scale plate motions (e.g., the north and south margins of the Tibetan plateau), and the plate-tectonically "neutral margins", which are less affected by plate scale process but may be tectonically contractional owing to the gravitationally-driven outward flows of the plateau material (e.g., the eastern margin of Tibetan plateau). Clearly, channel injection can, in principle, be the sole mechanism that thickens the crust in the transition zone of neutral margins, but there must be a component of tectonic contraction of the crust of the actively convergent margins. This distinction separates plateau transition zones into two classes, the actively convergent type modelled in Beaumont *et al.* (2001, 2004) and Vanderhaeghe *et al.* (2003) and the neutral type modelled by Clark & Royden (2000). The

three-dimensional models (Royden 1996, Shen *et al.* 2001) can address both types of boundary.

The two fundamentally different types of boundary raises the "chicken-and-egg" issue in regard to the role of channel injection in crustal thickening and the growth of plateaus. Can injection of channel material occur directly into normal continental crust, as modelled by Clark & Royden (2000), or must there be a precursory phase of tectonic thickening followed by thermal incubation to develop the hot, weak conditions under which channel injection will operate efficiently?

In this paper, successively more complete approximations to the evolution of a continental plateau and the adjacent transition zone by the channel injection mechanism are examined. The first two models, CI-1 and CI-2, largely ignore the thermal aspects of the problem. In CI-3 an associated thermal model is introduced which allows both the thickness and the temperature/viscosity of the channel to be predicted. The last part of the paper addresses the question of mechanical and thermal consistency by restricting the acceptable range of model parameter values to those thermal conditions for which the mechanics of channel injection will both operate efficiently and give results compatible with observations. This analysis also includes a comparison of the CI model with simplified models of viscous thickening (Fig. 1c) and plastic translation (Fig. 1d) of the crust.

The possible range of parameter values is large, therefore we restrict the models to those that produce similar geometries to those of Beaumont *et al.* (2004) for the transition zone at a similar time during their evolution. The range of consistent rheological and boundary conditions are then compared among models and with natural examples.

1 Channel Injection Theory

The simple shear thin sheet approximation (Medvedev and Podladchikov 1999, Lehner 2000) and mass balance (eq. 1) describe the flow in a linearly viscous, locally isostatically

balanced, crustal channel,

$$\begin{aligned} \frac{\partial S_2^+}{\partial t} + \Phi \frac{\partial q}{\partial x} &= 0 \ , \\ \frac{\partial h_2}{\partial t} + \frac{\partial q}{\partial x} &= 0 \ . \end{aligned} \tag{1}$$

The geometry and boundary conditions (Fig. 2) are as follows, S_2^+ is the upper boundary of the channel material, $\Phi = (\rho_m - \rho_c)/\rho_m$ is the isostatic amplification factor and ρ_m and ρ_c are respectively the densities of mantle and crust. The material flux $q(x)$ through the channel, thickness $h(x)$, assuming lithostatic pressure and uniform density of the crust, is

$$q = \int_{S_1^-}^{S_1^+} V_x dz = -\frac{\rho g h^3}{12\mu} \frac{\partial S_3}{\partial x} \ , \tag{2}$$

where S_1^+ and S_1^- are the boundaries of the channel, μ is the viscosity of the channel material, and S_3 is the upper surface of the crust. The variation in S_3 induces lateral pressure gradients which drive the Poiseuille flow. The horizontal velocity inside the channel is

$$V_x(z) = -\frac{\rho g (z - S_1^-)(S_1^+ - z)}{2\mu} \cdot \frac{\partial S_3}{\partial x} \ . \tag{3}$$

The general model of the channel injection (Fig. 2) assumes three zones in the crust. Material between S_2^+ and S_3 and between S_2^- and S_M is pre-existing crust above and below the channel, and the material in this zone moves only vertically and acts as a passive load. Material between S_1^+ and S_1^- is the channel material actively involved in the current flow. The material between S_1^+ and S_2^+, and between S_1^- and S_2^- is material that accreted to the crust from the channel, and is passive once accreted. Equations 1 and 2 can be solved for a range of assumptions concerning the channel thickness, $h(x)$ and the channel viscosity $\mu(x)$, as described in the next sections.

1.1 Channel Injection Model CI-1: Transition Zone with Uniform Property Channel

This model, in which h and μ are constants, was used by Clark & Royden (2000) to calculate channel flow in the plateau bounding transition zone and the results were applied

to the eastern flanks of the Tibetan plateau. In addition to the uniform thickness and viscosity they assumed that material accretes (freezes) to the channel walls as soon as it crosses $S_1^{\pm}$, thereby thickening the region between S_1^+ and S_2^+ and S_1^- and S_2^-. This material then acts as part of the passive overburden by applying its weight to create a pressure gradient along the channel. In this model the geometry of the channel does not change with time ($h = const$), even though the velocity field and topography do evolve. Eqs 1 and 2 can be combined for this case, and using $S_3 - S_2^+ = const$ (i.e. constant thickness of the initial crust above the channel) gives:

$$\frac{\partial S_3}{\partial t} = \frac{\partial S_2^+}{\partial t} = \frac{\Phi \rho g h^3}{12} \frac{\partial}{\partial x} \left(\frac{1}{\mu} \cdot \frac{\partial S_3}{\partial x} \right) . \tag{4}$$

Using the assumptions of Clark & Royden (2000), that the channel has constant viscosity and the flux into the model is constant, ($\mu = const$,$q_b = const$), eq. 4 can be solved analytically for the evolution of the upper surface:

$$S_3(x,t) = q_b \left[\sqrt{\frac{\alpha t}{\pi}} \exp\left(-\frac{x^2}{\alpha t}\right) - x \operatorname{erfc}\left(\frac{x}{\sqrt{\alpha t}}\right) \right] , \tag{5}$$

where $S_3(x, t = 0) = 0$ is the initial position of upper surface, $\alpha = \frac{\Phi \rho g h^3}{3\mu}$, erfc is the complementary error function, and t is time.

Based on this approach, Clark & Royden (2000) estimated the distribution of viscosity in putative crustal channels under the north, east, and southeast margins of the Tibetan plateau using the current topography of those margins (S_3). As they acknowledge, the results are, however, critically dependent on parameters that cannot be accurately estimated (i.e. the values of h and q_b) and whether h, q_b, and μ are actually constant. If uncertainties in these parameters are taken into account, the resulting estimates for channel viscosity, μ, can vary by orders of magnitude even when q_b is known because the control parameter α scales as h^3/μ. Therefore, an uncertainty in h of a factor of slightly more than 2 causes an order of magnitude uncertainty in μ.

Figure 3 illustrates a typical result for model CI-1. Assuming constant flux of material

into the system, $q_b = 10^{-6}$ m^3/s per m along strike (which is equivalent to average rate of 3.3 mm/y in a 10 km thick channel), results in elevating the plateau side of the transition zone to 5.5 km in 20 My. Although the results in Figure 3a were obtained for the special case of 10 km thick channel with $\mu = 3 \times 10^{20}$ Pa·s, exactly the same results can be achieved for 20 km thick channel with $\mu_{20} = 2.4 \times 10^{21}$ Pa·s, where the subscript indicates the assumed thickness of the channel in kilometers which yields this estimate of the viscosity.

While the results of Clark & Royden (2000) compare well with the topography of the chosen margins of the Tibetan plateau, there is a need to address additional questions that cannot be answered by channel injection model CI-1. For example, how is the flux q_b determined dynamically and would the available differential pressure drive this particular flux? How can this model of the transition zone be matched to the geometry of the plateau itself, and how are the overall dynamics of these two regions related?

1.2 Channel Injection Model CI-2: Constant Thickness, Variable Viscosity Channel

The approach of Clark & Royden (2000) can be combined with that of Royden (1996) which used a depth-dependent model of viscosity. Based on the assumption that temperature increases with depth in the crust and that viscosity correspondingly decreases, we propose a model in which the channel develops at the base of the upper crust (Fig. 4). In this model there is a step decrease in the channel viscosity when the centre of the channel, depth d, reaches a critical depth D^* (Fig. 4). This decrease can be interpreted to be the consequence of partial melting. Thus, viscosity in the channel is, $\mu = \mu(x, t, D^*)$, and the evolution of the system is described by the same eq. 4 as in the model CI-1 (Section 1.1). This model can address both the development of the transition zone ($d < D^*$) and the adjacent plateau ($d > D^*$).

The boundary flux q_b and viscosity $\mu(d)$ were chosen in a similar way to model CI-1

(Fig. 3) and to Clark & Royden (2000), so that the edge of plateau grows to a height of 5.5 km in 20 My, and also so that geometry of the transition zone is similar to geometry of the previous section (Fig. 3). Results display a plateau-like geometry of the orogen if the viscosity of the channel decreases by a factor of 100 under the plateau ($\mu(d > D^*) = \mu(d < D^*)/100$, Fig. 4b,c). The absolute value of viscosity can be estimated, as in the model CI-1, within the uncertainty of the control parameter h^3/μ (Fig. 4c). The dynamic link between plateau and its adjoining transition zone results in a more conservative estimates of the viscosity under the plateau ($\mu \approx 10^{18}$–10^{19} Pa·s) than ones presented in Clark & Royden (2000), where estimates based on the model CI-1 (Section 1.1) gave $\mu \approx 10^{16}$ Pa·s for equivalent h values.

Although the CI-2 model is very simple, it expresses a bulk behaviour similar to full 2D numerical models of plateau evolution (Vanderhaeghe *et al.* 2003). Once the plateau is established, it grows laterally and the geometry of the transitional zones remain self-similar (Fig. 4a) in a same manner noted by Vanderhaeghe *et al.* (2003). A simple kinematic analysis allows the rate at which the plateau edge advances, V_a, and the corresponding rate of plateau widening to be estimated. For the boundary conditions implemented here (i.e. the edge of plateau grows from 0 up to 5.5 km in 20 My) the edge of the plateau advances by the width of the transition zone in the same timescale ($V_a \approx 5$ mm/y). Mass balance relates V_a to the boundary flux by $q_b = V_a \Delta H_c$, and thus

$$V_a = q_b / \Delta H_c \approx const \tag{6}$$

where $\Delta H_c = H_{cp} - H_{c0} \approx const$ is the difference in the crustal thickness between the foreland and the plateau. Although the lateral variations of the plateau crustal thickness are small, the plateau crust must thicken internally (Fig. 4a) to drive the sub-plateau channel, because the rate of flow in the channel is proportional to local slope of topography. This requirement, however, is an artifact of the thin sheet approximation used here to describe the system. Beaumont *et al.* (2004) describes channel flow under a nearly flat

plateau using full 2D numerical calculations for which the driving force for the channel flow is not the local, but global changes in topography. We therefore simplify CI-2 model and assume constant thickness plateau crust, $H_{cp} = const$, and, correspondingly, $\Delta H_c = const$ in subsequent analysis.

V_a is not a material velocity, nor is it associated with the motion of any physical part of the system. The self-similar evolution of plateau is similar to the propagation of a kinematic wave such that the evolution of the topography in the transition zone can be expressed as $S_3(x,t) = S_3(x + V_a t)$. We use this property and assume that other model parameters also evolve in the form of a laterally propagating kinematic wave, such that in our thermal model (Appendix).

Similar geometry and dynamics of growth (5.5 km over 20 My) can be obtained for CI-1 and CI-2 models (Fig. 5) only if the viscosity of the channel under the transition zone in the model CI-2 is approximately 3 times smaller than in the model CI-1. The model CI-2 also requires a four times higher boundary flux into the system. The discrepancy is caused by an oversimplification in the model CI-1, which does not account for the kinematics of the advancing plateau. Building the plateau margin comprises two processes, first the development of the transition zone as in the model CI-1, and second the conversion of the margin to plateau, which is the process that requires the extra material flux. In this regard the model CI-2 is more complete than CI-1.

The kinematic connection between the transition zone and the plateau edge in the model CI-2 also results in a time-dependent flux into the transition zone at a fixed location even though the boundary flux q_b is a constant. Under the plateau, where the thickening rate is negligible, the flux in the channel $q \approx q_b = const$. The channel material flux then decreases across the transition zone to zero at the toe. Thus, the model CI-1 assumption of the constant flux into the transition zone cannot be combined with the plateau advancing with the constant rate V_a.

1.3 Channel Injection Model CI-3: Temperature-Dependent Channel Properties

While the resulting geometry of the model CI-2 looks realistic (Fig. 4), we question whether the physical foundation of the model is correct. Is depth a good proxy for temperature in determining channel properties? Would a better model based on the thermal evolution of the crust result in different channel properties and flow regimes.

Vanderhaeghe *et al.* (2003) compared depth- and temperature-dependent representations of crustal viscosity in models of plateau evolution. Although the topographic shape of resulting plateau can be similar for both rheologies, the internal structure of the plateau crust is substantially different. In the model in which viscosity decreases with depth (see also Royden 1996, and Shen *et al.* 2001), a low viscosity weak layer of constant thickness develops below the plateau and is reflected by the flat topography of the plateau. In contrast, the temperature-dependent viscosity model of the crust results in large, up to 20 km variations in the thickness of the low viscosity weak layer and, consequently, inversely correlated variations in the thickness of the overlying upper, strong and cold, layer (Vanderhaeghe *et al.* 2003). The geometry of the weak crustal layer determines the structure of the channel flow in the crust, therefore, we can expect different interactions between the overburden and the channel for the depth- and temperature-dependent models.

Here we combine the model CI-2 with an approximate thermal model (Appendix) to analyse the evolution of the plateau and the transition zone when the viscosity and the geometry of the channel is temperature dependent. We assume that instead of a critical depth, D^*, the channel viscosity decreases when the channel temperature reaches critical value, T^*, corresponding to the onset of significant melt weakening. The channel thickness, initially h_0, increases to include the mid- and upper crust where $T > T^*$, but not the lower crust which is assumed to be in granulite facies and not subject to melting. This model approximates radioactive self-heating, partial melting, weakening of crustal material, and

the consequent increasing region of actively deforming low-viscosity crust, with the critical temperature $T^* = 750^\circ$ C, chosen to represent the effect of muscovite dehydration melting (Johannes & Holtz 1996).

The Associated Thermal Model (Appendix), which calculates the one-dimensional vertical thermal evolution, and the self-similar widening of the plateau (Section 1.2), is used to determine the horizontal distribution of temperature $T(x, z, t) = T(z, t - x/V_a)$. To make the results of CI-2 and CI-3 comparable, we chose the thermal parameters of the model (Table 1) so that the mid-channel temperature also reaches the critical value after 20 My of transition zone thickening.

The results (Fig. 6) look similar to those of CI-2 (Fig. 4), but in this case the channel becomes thicker as the plateau crust self-heats and approaches a steady thermal state. The thermal dependence of the channel geometry provides an independent self-consistent measure for thickness of the channel, whereas in models CI-1 and CI-2 the choice of channel thickness is arbitrary. Comparison of the model topographies (Fig. 7) shows that a similar geometry to that of CI-2 is obtained for CI-3 with a smaller decrease in viscosity because the channel thickness increases from its initial value, h_0, in CI-3, but remains constant in CI-2 (compare figures 4 and 6).

2 Thermal and Rheological Consistency

The previous section presented the CI-3 model, which combines mechanical and thermal models. These are separable into the two parts. The next step is to analyse the relationship between these two parts for internal consistency, and consistency with natural systems. We first discuss the correlation between melt weakening, its consequences for the boundary between the transition zone and the plateau, and then examine the effect of temperature variations along the channel in the transition zone. Lastly, we ask whether the viscosity of channel material implied by the model results is consistent with laboratory measurements

of quartz-controlled rheologies.

2.1 Criteria for the Initial and Transient Consistency of the Thermal and Mechanical Models

Three criteria can be used to analyse consistency between the mechanical and thermal models.

1. Initial Conditions: if channel flow is the mechanism that tectonically thickens the crust, the temperatures in the crust must be high enough, and the associated viscosity must be low enough, to allow viscous channel flow to occur under the initial ambient conditions.

2. Temperature Change: the temperature change in each crustal column, while it is in the transition zone, should be such that the final temperature meets the requirements for the channel viscosity to decrease by melt weakening so that the transition to the plateau topography will occur.

3. Timescale of Temperature Change: the timescale for the increase in temperature and the onset of melt weakening of the transition zone must agree with that of the mechanical thickening, so that the mechanical and thermal plateau transitions are compatible.

The first criterion addresses the initial thermal state of undeformed crust. Our reference model (Table 1, Fig. 6) with $h_0 = 10$ km is consistent because the temperature at the top of the channel is 400°C (Fig. A2) and the threshold for viscous creep in quartz-controlled crust is approximately 300°C. Moreover, any equivalent foreland crust is consistent if the radioactive heat production is 0.75 μW/m^3 or higher. However, a requirement for a thicker channel, e.g. $h_0 = 15$ km is marginally too cold (290°C at the top of the channel) unless the thermal parameters are changed. Increasing radioactive heat production would, for

example, require A=5.4 μW/m^3 for the corresponding channel to be 20 km thick.

The second criterion determines whether thickening the crust results in efficient heating. Crustal thickening results in transient heating, but this occurs with a characteristic timescale often longer than the timescale for mechanical thickening. Comparison of the increase of the temperature at the base of the crust versus the timescale for crustal thickening (Fig. 8) shows that fast mechanical thickening (timescale <10 My) only results in moderate increases in temperature so that both mechanisms, CI and PS (pure shear, Appendix), are ineffective. For thickening timescales that are very long (>40 My), both mechanisms predict significant heating. At intermediate timescales, which are common in natural orogens, CI is seen to be a more efficient mechanism for crustal heating than PS.

The longer term differences are a consequence of the relative contributions from radioactivity. Pure shear thickens the crust uniformly producing a 44 km thick high radioactivity layer (this layer is only 22 km thick in CI), but the crust self-heats slowly redistributing heat conductively. Channel injection heating is more efficient for thickening timescales less than 40 My because CI injects hot material from lower in the crust and channel flow advects heat from hot crust beneath the plateau (Appendix).

The third consistency criterion concerns the timing of the thermal evolution in the transition zone and requires that the base of the crust be close to the melting temperature at the time the transition zone transforms into a plateau. This transformation is interpreted to be a consequence of the decrease in viscosity owing to melt weakening. Figure 9a shows the temperature predicted at the depth of the middle of the channel for the CI-3 model after 20 My of crustal thickening as a function of the radioactivity of the upper crust, A_1, and thermal capacity, C_p, (other parameter values are as given Table 1). High values of A_1 and low values of C_p produce temperatures compatible with the onset of melting. Equivalent results for the PS model (Fig. 9b) are similar but the crust is colder for the same parameter values. Rather than analysing for consistent models we reject inconsistent ones

on the basis that melting most likely occurs in the temperature range 700–750°C (Johannes & Holtz 1996). Models that do not achieve this temperature range in 20 My, and models that achieve these temperatures too quickly, were rejected leaving those with parameters in the range shown by the two shaded bands (Fig. 9c) for the CI-3 and PS models. Similar plots can be made for other combinations of parameters and duration of thickening.

Particular cases can also be analysed for consistency. For example, parameter values used by Beaumont *et al.* (2001, 2004) for Himalyan-Tibetan models are inconsistent with thickening by CI-3 but consistent with PS (Fig. 9c). This result also agrees with their numerical model results which showed PS thickening in the transition zone and channel flows only penetrating this region when there is significant erosion. The parameters used by Babeyko *et al.* (2002) to model the Altiplano are incompatible with both modes of thickening on the 20 My timescale and would require a minimum 35 My interval of thickening for CI to operate and 45 My for PS. If the Altiplano crust is expanding outward and thickening the transition zone it must have an additional source of heat not considered in our CI and PS models.

2.2 Criteria for the Rheological Consistency of the Channel below the Transition Zone

In this section we investigate under what circumstances channel injection is consistent with laboratory measurements of the rheological properties of quartz-rich rocks. Natural plateaus usually exhibit an abrupt boundary between the transition zone and the plateau, which we have interpreted to reflect a significant step decrease in channel viscosity related to the onset of partial melting (Fig. 6). An alternative explanation is that the viscosity variation of quartz-rich crust with temperature and strain rate is sufficient to explain the abrupt plateau-edge transition without melt weakening. The large uncertainty in the effective viscosity of quartz-rich rocks is seen from Figure 10, which shows laboratory data

(Gleason & Tullis 1995, Table 3) plotted as effective viscosity versus temperature. The plot differs from the usual ones of this type in that the assumed strain rate is not constant but varies from 10^{-15} s^{-1} to 10^{-13} s^{-1}, as shown, to reflect the anticipated variation in strain rate between the foreland end of the channel, where temperatures may be as low as 300–400°C, and the plateau end of the transition zone, where temperatures may reach 700–800°C, and the strain rates are larger.

The results show that the extrapolated effective viscosity estimates are approximately 10^{21} Pa·s with a factor of 3 uncertainty at 400°C, and 10^{19} Pa·s at 750°C, but with a much larger, approximately factor of 10, uncertainty. If we eliminate the two lowest viscosity estimates based on the reliability of the laboratory measurements as discussed by Gleason & Tullis (1995), we predict that for the temperature range 400–750°C, calculated for the channel beneath the transition zone, the associated viscosities should correspondingly vary from 10^{21} Pa·s to 10^{19} Pa·s. Figure 11 shows the plateau-edge geometry for this choice of viscosity variation compared with that predicted by the CI-3 model with constant viscosity in the transitional channel and an abrupt decrease in the viscosity at the plateau edge. Despite the admittedly large uncertainties, it can be seen that the geometry based on the extrapolated laboratory data, and not including melt weakening, fails to predict the abrupt plateau-edge geometry. In addition, this model predicts that the topography increases steeply at the toe, much more steeply than the CI-3 model (Fig. 11). This steepness is because channel flow is very inefficient at viscosities high than 10^{20} Pa·s, which suggests that normal crustal thickening at the foreland end of the transition zone is not rheologically consistent with the channel injection model and that an alternative mechanism needs to be considered.

A similar question of rheological consistency arises in regard to the Clark & Royden (2000) estimate of the channel viscosities of 10^{18} Pa·s for a 1500 km wide region of the southeast Tibetan plateau margin south of the Sichuan Basin. Such low viscosities require

temperatures of approximately 800°C even for the lower effective viscosity extrapolations of the laboratory data (Fig. 10). The results imply that the channel injection explanation for crustal thickening only applies if the crust in this region was already anomalously hot prior to channel injection, which raises the related question whether it was already anomalously thick.

3 Behaviour of the Upper Crust

We complete the analysis with a preliminary description of other mechanisms, Viscous Thickening, VT, and Plastic Translation, PT (Fig. 1c and d), which may also contribute to deformation and crustal thickening of the transition zone but differ from Channel Injection.

3.1 Viscous Thickening Model

The CI models assume that crust above the channel is much stronger than channel material and therefore does not deform during injection. However, if this is not correct the deformation can instead be evenly distributed in the transitional crust. Simple models of this type treat the deformation as viscous, are based on the simple shear thin sheet approximation (e.g., Buck and Sokoutis 1994, Royden 1996, Medvedev 2002), and assume that the upper surface of the crust is deformable and stress free. The remaining boundary conditions are the same as those for the CI model.

The VT model is of this type (Fig. 12) and the mass balance gives

$$\frac{\partial S_3}{\partial t} + \Phi \frac{\partial q_v}{\partial x} = 0 \, , \tag{7}$$

which is similar eqs 1 and 2, except the corresponding flux

$$q_v = -\frac{\rho g h_2^3}{3\mu} \frac{\partial S_3}{\partial x} \, . \tag{8}$$

results from integration of the velocity profile, which is

$$V_x(z) = -\frac{\rho g (z - S_1^-)(h_2 + S_1^+ - z)}{2\mu} \cdot \frac{\partial S_3}{\partial x} \tag{9}$$

for a uniformly viscous crust and assuming lithostatic pressure.

The resulting system of equations is similar to those for the CI model (eqs 1 – 3), except for the denominator 3, instead of 12, in the expressions for the fluxes. This difference occurs because the upper surface in the VT model is free to deform. Note also that the VT equations are non-linear (h_2 is a linear function of S_3) and cannot be solved analytically. The model result (Fig. 12) is shown for the viscosity 1.5×10^{22} Pa·s which produces the same transition zone geometry as the CI-2 and CI-3 models with channel material viscosity of 10^{20} Pa·s.

The difference of two orders of magnitude in the viscosity required to produce the same topography for the transition zone demonstrates the sensitivity of the behaviour to the mode of deformation. This result implies that for natural examples the type of deformation must be known, in addition to the geometry, before the viscosity can be accurately estimated. An example is the very wide (approx. 1500 km) transition zone southeast of the Sichuan basin for which Clark & Royden (2000) estimated a viscosity of 10^{18} Pa·s based on the CI model. The corresponding estimate from the VT model is 2×10^{20} Pa·s, which may be more realistic if contraction at the surface cannot be ruled out.

3.2 Stability of the Upper Crust

The last mode of deformation in the transition zone considers the plastic (brittle) failure and translation, PT, of the crust above the channel injection zone. Here we estimate the stability of the upper crust, which allows us to distinguish when the CI and PT modes will operate. Lehner (2000) considers the stability of frictional overburden coupled to a viscous substratum and uses the thin sheet approach for the channel flow (eq 1) and the small angle approximation for the overburden. Gemmer *et al.* (2004) present a simplified version of the theory for systems with constant thickness channels and they also derive an expression for the velocity when the crust is unstable. The results are in good agreement with full 2D

numerical calculations.

Consider the forces acting on a block of the crust above the channel in the transition zone (Fig. 13, area surrounded by bold line). The horizontal balance of forces is:

$$F_p - F_0 - F_{nx} + F_\tau = 0 \ , \tag{10}$$

where F_p and F_0 are the normal forces acting on the block from the edge of plateau and from the foreland respectively, F_τ is the traction on the base of the block produced by the Poiseuille flow in the transitional channel, and F_{nx} is the horizontal component of the buoyancy force. If the forces in eq. 10 cannot be balanced, the block becomes unstable and starts to move. The forces can be estimated in the following ways. The wedged shaped block, thickness $h_w(x)$, has two parts, an upper uniform frictional-plastic layer, thickness h_b, and the lower approximately triangular viscous region above the channel and below the plastic layer. Therefore,

$$F_p = \int_{S_1^+(x_p)}^{S_3(x_p)} \sigma_{xx}\, dz = F_{pb} + F_{pv} \tag{11}$$

where, F_{pb} and F_{pv} are the integrals of the horizontal stress within the plastic and viscous parts, respectively at $x = x_p$. Integration of the stress under the small angle assumption for the geometry of the block, and assuming that the principal stresses are horizontal and vertical and the pressure is equal to the lithostatic pressure gives (Gemmer et al. 2004): $F_{pb} > F_p^* = \rho g h_b^2 k/2$ and $F_{pv} = \rho g(h_{wp}^2 - h_b^2)/2$. $k = (1 - \sin\phi)/(1 + \sin\phi)$ is the coefficient of passive earth pressure (Lehner 2000), where ϕ is the internal angle of friction of the overburden, and $h_{wp} = h_w(x_p)$ is the thickness of the system at the edge of plateau. F_p^* is the limiting value of F_{pb} when the system is on the verge of failure, or has failed. Under the equivalent assumptions, $F_0 < F_0^* = \rho g h_b^2 k^{-1}/2$.

The horizontal component of the normal stress at the base of the system can be calculated following Medvedev and Podladchikov (1999) by estimating the buoyancy by

integrating the pressure along the base of the block,

$$F_{nx} = \int_{x_o}^{x_p} \rho g h_w(x) \frac{\partial S_1^+(x)}{\partial x}\, dz = \frac{\rho^2 g}{2\rho_m} \int_{x_o}^{x_p} \frac{\partial h_w^2}{\partial x}\, dz = \frac{\rho^2 g}{2\rho_m} \left(h_{wp}^2 - h_b^2\right) \ . \tag{12}$$

Here we use the constraint that the boundary S_1^+ is parallel to the base of the crust (Fig. 13), and the Airy isostatic condition,

$$\frac{\partial S_1^+}{\partial x} = \frac{\rho}{\rho_m} \cdot \frac{\partial h_w}{\partial x} \ , \tag{13}$$

where ρ_m is the density of the lithospheric mantle (Table 1). The traction force from the viscous flow in the channel is determined by integrating the basal drag caused by the channel injection along the length the block (Gemmer *et al.* 2004):

$$F_\tau = \frac{\rho g h}{2} \left(S_3(x_p) - S_3(x_0)\right) = \frac{\rho \Phi g h}{2} \left(h_{wp} - h_b\right) \ , \tag{14}$$

where Φ is the isostatic amplification factor (Table 1). Substitution of the force estimates into eq. 10 gives the stability condition for the system:

$$h_b^2 \left(k - k^{-1}\right) + \Phi \left(h_{wp}^2 - h_b^2\right) + \Phi h \left(h_{wp} - h_b\right) < 0 \ . \tag{15}$$

Equation 15 can be solved for the critical limiting value of ϕ, ϕ^* (below which the block becomes unstable) using the geometry (Fig. 6) and properties (Table 1) of our reference model. Here we use h_b =15 km, based on the depth to the 400°C isotherm calculated using the associated 1D thermal model (Appendix) and shown in Figure A2. Crust below this level will almost certainly be viscous. If h_{wp} = 40 km, ϕ^*= 21.5°. The block will be unstable if $\phi < \phi^*$. It is also worth noting that erosion which occurs sufficiently rapidly to reduce the thickness of the frictional-plastic layer will tend to destabilize the system by reducing F_p^* and/or F_0^*. This effect is seen in the numerical models (Beaumont *et al.* 2004, Fig. 7) and leads to the transition from channel flow beneath stable plateau and transitional crust to unstable outward flow of the upper crust together with the channel. For example, for the current reference model a reduction of the frictional-plastic layer

thickness to 10 km would render the block unstable for $\phi = 21.5°$ and requires an increase to $\phi^* = 37°$ if the system is to remain stable.

If the system becomes unstable, the overburden fails, the block glides outward with velocity V_C, and the force balance (eq. 10) becomes

$$F_p^* + F_{pv} - F_0^* - F_{nx} + F_\tau - F_C - F_V = 0 \tag{16}$$

where the forces F_{pb} and F_0 are replaced by their limiting values because the frictional-plastic overburden has failed. $F_C = \mu L_C V_C / h$, is an additional force owing to the basal drag of the Couette flow in the viscous channel on the overburden (Gemmer *et al.* 2004), and $L_C = x_p - x_0$. F_V is the additional viscous force that results from the extension of the viscous crust above the channel at the edge of the plateau. This force can be estimated by assuming that the triangular region necks viscously with a horizontal length scale L_n, which gives

$$F_p = \int_{S_1^+(x_p)}^{S_2^+(x_p)} 2\mu_w \frac{V_C}{L_n}\, dz = 2\mu_w (h_{wp} - h_b) \frac{V_C}{L_n} \,, \tag{17}$$

assuming that the triangle block has a uniform viscosity μ_w in the region that necks.

The following results are obtained assuming $h_b = 15$ km, $L_C = 100$ km, $L_n = 30$ km, and $\mu_w = 10^{22}$ Pa·s, and using other parameters values from Table 1. The maximum velocity $V_C = 8$ mm/y occurs when $\phi = 0°$, and ranges from 6 mm/y ($\phi = 5°$), through 5 mm/y ($\phi = 9°$), to 2.75 mm/y ($\phi = 15°$). These results demonstrate that passive plateau margin transition zones can be close to extensional failure and the outward flow velocities can be significant if the viscosity of the crust above the channel at the plateau margin is approximately 10^{22} Pa·s. The outward flow could still be significant on geological timescales even if this viscosity were an order of magnitude higher.

4 Conclusions

1. Simple modelling has been used to improve our understanding of the first-order controls on the growth of continental plateaus and the interactions that occur within the transition zone at the plateau margin. The simplified approach of this study also helps us to gain more insight into the results of numerical models which produce realistic looking geometries, but are difficult to interpret in terms of the basic physical controls (Beaumont *et al.* 2001, 2004; Jamieson *et al.* 2004).

2. The Three Channel Injection, CI, models. We developed successively more complete approximations to the evolution of a continental plateau and adjacent transition zone by the CI mode. CI-1, the simplest approximation (based on Clark & Royden 2000), assumes a constant viscosity and thickness channel in which excess material accretes in zones above and below the channel. While the predictions of this model compare well with some natural examples, this model does not consider relations between plateau and transition zone. CI-2 includes a decrease in channel viscosity, predicted to occur on melt weakening or at high temperatures, when the crustal thickness exceeds a critical value, D^* This model completes the connection between plateau and transition zone, but relies on the arbitrary chosen critical thickness of the crust. CI-3 is more realistic and considers the channel viscosity and thickness to be temperature dependent. CI-3 includes an associated thermal model which accounts for radioactive self-heating of the transition crust and for the heat advection as channel material flows from beneath the plateau. CI-3 demonstrates self-consistent plateau widening if the channel viscosity decreases when its temperature exceeds the critical value T^*.

The simplicity of the models allows analytical solutions for some cases and provides direct estimates of the parameters that control channel flow. Acceptable results for the topography of Tibet, for example, are achieved by CI-3 model when the channel viscosity is in the range 10^{18}–10^{19} Pa·s beneath Tibet and 10^{19}–10^{22} Pa·s beneath the adjacent areas

and the critical temperature for the onset of partial melting is in the range 700–750°C. These values agree with those determined from fully coupled thermal-mechanical models.

3. Consistency of Thermal and Mechanical Models. The first thermal consistency test requires the initial thermal-viscous structure of the crust to be compatible with crustal thickening by channel injection. The second thermal consistency test asks whether the temperature reaches the melting point, thereby initiating melt weakening, at the appropriate place and time. Comparison of the thermal evolution of CI-3 with a model in which transitional crust tectonically thickens uniformly (PS) shows that CI is a much more effective mechanism for heating the transitional crust. The third, transient, thermal consistency test assesses whether the development of the melting conditions in the transitional crust coincides with the end of thickening. Premature melt weakening will, for example, result in the flattening the transitional zone topography before it reaches the level of the plateau, and that is incompatible with lateral growth of plateau. The requirement for consistency significantly restricts the range of compatible parameter values.

4. Rheological Consistency. Rheological consistency compares the model predictions of channel viscosity for the transitional crust with viscosity estimates from laboratory experiments. Modelling of wide (1.5–2$\times 10^3$ km) transitional zones, for example, with the CI-3 model requires the channel viscosity to be about 10^{19} Pa·s, which is incompatible with laboratory data for quartz-based rheologies without "melt weakening".

5. Viscous Thickening, VT, and Plastic Translation, PT, of the Transitional Crust. The compatibility of the CI models, which assume only vertical passive motion of the upper crust, was compared with possible VT and PT deformation of the upper crust. Predicted CI-3 topography of the transition zone can be reproduced by viscous thickening of the crust, but the corresponding VT model estimates of the crustal viscosity are up to two orders of magnitude higher than those for CI. This result indicates that topography alone is not a sufficient basis from which to estimate crustal viscosity. The mode of deformation

must also be known. Stability estimates for the failure and outward flow of the plateau margin, PT mode deformation, indicate that neutral plateau transition zones may be close to failure by plastic translation of the crust above a channel.

References

Babeyko, A. Yu., Sobolev, S. V., Trumbull, R. B., Oncken, O. & Lavier, L. L. 2002. Numerical models of crustal scale convection and partial melting beneath the Altiplano-Puna plateau. *Earth Planetary Science Letters*, **199**, 373–388.

Beaumont, C., Jamieson, R. A., Nguyen, M. H. & Lee, B. 2001. Himalayan tectonics explained by extrusion of a low-viscosity channel coupled to focused surface denudation. *Nature*, **414**, 738-742.

Beaumont, C., Jamieson, R. A., Nguyen, M. H. & Medvedev, S. 2004. Crustal Channel Flows: 1. Numerical models with applications to the tectonics of the Himalayan-Tibetan Orogen. *Journal of Geophysical Research*, **109**, B06406, doi: 10.1029/2003JB002809.

Bird, P. 1991. Lateral extrusion of lower crust from under high topography, in the isostatic limit. *Journal of Geophysical Research*, **96**, 10275–10286.

Buck, W. R. & Sokoutis, D. 1994. Analogue model of gravitational collapse and surface extension during continental convergence. *Nature*, **369**, 737–740.

Clark, M. K. & Royden,L. H. 2000. Topographic ooze: Building the eastern margin of Tibet by lower crustal flow. *Geology*, **28**, 703–706.

Gemmer L, Ings, S., Medvedev, S. & Beaumont, C. 2004. Salt tectonics driven by differential sediment loading: Stability analysis and finite element experiments. *Basin Research*, **16**, 199-218, doi: 10.1111/j.1365-2117.2004.00229.x.

Gleason, G. C., & Tullis, J. 1995. A flow law for dislocation creep of quartz aggregates determined with the molten salt cell. *Tectonophysics*, **247**, 1–23.

Jamieson, R. A., Beaumont, C., Medvedev, S. & Nguyen, M. H. 2004. Crustal channel flows: 2. Numerical models with implications for metamorphism in the Himalayan-Tibetan Orogen. *Journal of Geophysical Research*, **109**, B06407, doi:10.1029/2003JB002811.

Johannes, W. & Holtz, F. 1996. *Petrogenesis and experimental petrology of granitic rocks.* 335 p., Springer-Verlag, Berlin.

Kaufman, P. S. & Royden, L. H. 1994. Lower crustal flow in an extensional setting: Constraints from the Halloran Hills region, eastern Mojave Desert, California. *Journal of Geophysical Research*, **99**, 15723–15739.

Lehner, F. K. 2000. Approximate theory of substratum creep and associated overburden deformation in salt basins and deltas. In Lehner, F. K. & Urai, J. L. (eds.) Aspects of Tectonic Faulting, Springer-Verlag, Berlin, 21–47.

Medvedev, S. 2002. Mechanics of viscous wedges: Modeling by analytical and numerical approaches. *Journal of Geophysical Research*, **107**, B6, 10.1029/2001JB000145.

Medvedev, S. E. & Podladchikov, Yu. Yu. 1999. New Extended Thin Sheet Approximation for Geodynamic Applications – II. 2D examples. *Geophysical Journal International*, **136**, 586–608.

Royden, L. H. 1996. Coupling and decoupling of crust and mantle in convergent orogens: Implications for strain partitioning in the crust. *Journal of Geophysical Research*, **101**, 17679–17705.

Shen, F., Royden, L. H. & Burchfiel, B. C. 2001. Large-scale crustal deformation of the Tibetan Plateau. *Journal of Geophysical Research*, **106**, 6793 - 6816.

Vanderhaeghe, O., Medvedev, S., Beaumont, C., Fullsack, P. & Jamieson, R. A. 2003. Evolution of orogenic wedges and continental plateaux: insights from crustal thermal-mechanical models overlying subducting mantle lithosphere. *Geophysical Journal International*, **153**, 27–51.

Appendix: The Associated Thermal Model

This appendix develops an approximate 1D vertical model for the the temperature in crust that is thickened by channel injection. It is used in conjunction with Channel Injection models (Sections 1.3 and 2) to investigate how channel flows may develop when viscosity depends on crustal temperature. To emphasise the role of the mode of thickening, we compare CI mode with the model in which the upper and middle crust thickened by pure shear, PS, mode.

Vanderhaeghe et al. (2003) demonstrated that the 2D cross-sectional thermal evolution of plateau crust can in some circumstances be explained approximately by the analysis of a reduced vertical 1D thermal problem. We use the same approach here. Based on the result that vertical temperature variations are much larger than horizontal ones (as determined from the first and second spatial derivatives from 2D calculations), term 6 of the 2D thermal equation,

$$\frac{\partial T}{\partial t} = \frac{A}{\rho C_p} - V_z \frac{\partial T}{\partial z} + \kappa \frac{\partial^2 T}{\partial z^2} - V_x \frac{\partial T}{\partial x} + \kappa \frac{\partial^2 T}{\partial x^2} \ , \tag{A1}$$

may be neglected. This assumption is also in agreement with thin-sheet character of our mechanical model, where the horizontal variations are assumed to be small. In eq. A1, T is the temperature, t is time, A is the rate of radioactive self-heating, C_p is the specific heat at constant pressure, V_z and V_x are vertical and horizontal components of velocity, $\kappa = K/(\rho C_p)$ is the thermal diffusivity, and the numerical values of the parameters are given in Table 1.

Pure Shear Model A specific example of pure shear crustal thickening is solved. This model is then used as a reference for comparison with the CI models. We assume that upper and middle crust is thickened at a uniform rate by a factor of 2.2 in 20 My resulting in a total crustal thickness of 65 km, at which time the crust is assumed to become stable plateau crust (Fig. A1). In addition to above simplification noted above, in this model we also neglect the horizontal advection (term 5, eq. A1) on the basis that this term is much smaller than the vertical advection (term 3, eq. A1) because both velocity components are small but the vertical temperature gradient is larger. The simplified equation is solved numerically and Figure A1 shows the result for the reference model. Note that the upper, highly radioactive part of the crust thickens significantly from initial 20 km to 44 km.

Channel Injection Model CI-3 To apply the thermal model to channel injection in the CI-3 model we use the self-similar nature of the lateral growth of the plateau (Sections 1.2 and 1.3). We assume that the temperature field also evolves in a self-similar manner, that is, $T(x, z, t) = T(x + V_a\Delta t, z, t + \Delta t)$. This implies that during steady-state plateau growth, the vertical thermal structure migrates laterally with the same velocity as the plateau edge, V_a (eq. 6). Furthermore, in CI-3 the horizontal advection of heat cannot be neglected because V_x in the channel may be large. The self-similarity of the temperature profile gives

$$\frac{\partial T}{\partial x} = -\frac{1}{V_a} \cdot \frac{\partial T}{\partial t} \approx -\frac{1}{V_a}\left(\frac{A}{\rho C_p} - V_z\frac{\partial T}{\partial z} + \kappa\frac{\partial^2 T}{\partial z^2}\right) , \tag{A2}$$

where the first equality results from

$$\frac{\partial T}{\partial t} = \lim_{\Delta t\to 0}\frac{T(x,z,t+\Delta t)-T(x,z,t)}{\Delta t} = \lim_{\Delta t\to 0}\frac{T(x,z,t+\Delta t)-T(x+V_a\Delta t,z,t+\Delta t)}{\Delta t} = -V_a\frac{\partial T}{\partial x} . \tag{A3}$$

The approximate equality in eq. A2 is the zeroth-order approximation of the horizontal temperature gradient in the system. Combining eqs A1 and A2 gives the higher order approximation for the thermal evolution of crust thickened by channel injection:

$$\frac{\partial T}{\partial t} = (1 + \theta_c)\left(\frac{A}{\rho C_p} - V_z\frac{\partial T}{\partial z} + \kappa\frac{\partial^2 T}{\partial z^2}\right) . \tag{A4}$$

Here, θ_c is the channel heat advection coefficient. It is zero outside of channel and $\theta_c = V_x/V_a$ inside the channel. It can be seen that the horizontal channel flux accelerates the thermal evolution in the vicinity of the channel by a factor $(1 + \theta_c)$. The distribution of θ_c can be found from the mass balance. First, eq. 1 and self-similarity of geometry of the transition zone give

$$\frac{\partial q_p}{\partial x} = -\frac{\partial h_2}{\partial t} = V_a \frac{\partial h_2}{\partial x} \ . \tag{A5}$$

The requirement that $q_p = 0$ in the undeformed foreland allows integration of eq. A5:

$$q_p = V_a(h_2 - h_0) \ , \tag{A6}$$

where h_0 is the initial thickness of the channel. In addition, the depth dependence of the horizontal velocity eq. 3 can be expressed via flux in the channel, q_p, using eq. 2:

$$V_x(z) = \frac{6q_p}{h^3}(z - S_1^-)(S_1^+ - z) \ . \tag{A7}$$

Combining eqs A6 and A7 we obtain channel heat advection coefficient inside the channel of thickness h:

$$\theta_c = \frac{V_x}{V_a} = \frac{6(h_2 - h_0)}{h^3}(z - S_1^-)(S_1^+ - z) \ . \tag{A8}$$

We solve eq. A1 (for the pure-shear model) and eq. A4 (for the CI-3 model) numerically using a Lagrangian approach and a finite-difference approximation. The 1D mesh consists of 200–300 grid points with variable density of the mesh (more dense in the upper and mid-crust). The bottom boundary condition (heat flux, q_m) is set initially at the depth of 95 km.

To illustrate the results we consider two model properties, the temperature evolution for a point located 5 km above the base of the upper crust (Fig. A2a), and the time when the temperature at this location reaches the critical value (Fig. A2a,b). The model behaviour will be consistent with the channel injection behaviour and melt weakening to form a

plateau if, at 20 My, the lower part of the upper crust reaches a high enough temperature, approx 750°C ($\Delta t = 0$, meaning the temperature is reached a the specified 20 My time). Significant lead ($\Delta t < 0$) or lags ($\Delta t > 0$) in the time this condition is achieved implies the thermal evolution is not consistent with the mechanical model which assumes that the transition to a plateau occurs at 20 My. The same consistency conditions can be applied to the model of plateau in which the transition zone thickens by pure shear mode (Fig. A1).

We consider two types of thermal consistency. The CI-3 model (Sections 1.3) requires an exact match between the mechanical and thermal models ($T^* = 750$°C, $\Delta t = 0$). However, in the sensitivity analysis (Section 2.1) our uncertainty in the in the critical temperature is acknowledged and we consider a range, 700–750°C.

Table 1. *Parameters of the reference model*

Variable	Definition	Values
	Geometry	
H_c	Thickness of the model crust:	
H_{c0}	initial crustal thickness	35 km
H_{cp}	crustal thickness at the edge of plateau	65 km
h_2	Thickness of deformable part of the crust(Fig. 2)	10→40 km
h	Thickness of the crustal channel in the CI model (Fig. 2)	$h_0 = 10$ km
d	Depth of the middle of the channel	$d_0 = 20$ km
h_3	Thickness of the lower, undeformable crust (Fig. 2)	10 km
S_{3p}	Uplift of topography at the plateau edge ($S_{30} = 0$, Fig. 2)	5.5 km
	Mechanical parameters	
t^*	Thickening time	20 My
g	Acceleration due to gravity	9.8 m/s^2
ρ	Density of the crust	2700 kg/m^3
ρ_m	Density of the lithospheric mantle	3300 kg/m^3
Φ	Isostatic amplification factor $(1 - \rho/\rho_m)$	0.18
μ	Viscosity of the channel material	*variable* [Pa·s]
	Thermal parameters	
$T(x, z, t)$	Temperature (eq. A1)	[°C]
T_{top}	Temperature on the top surface (boundary condition for eq. A1)	0°C
T^*	Critical temperature (Fig 6)	750°C
q_m	Mantle heat flux (boundary condition for eq. A1)	20 mW/m^2
C_p	Heat capacity (eq. A1)	750 J/kg/K
K	Thermal conductivity (eq. A1)	2 W/m°K
κ	Thermal diffusivity (= $K/\rho C_p$, eq. A1)	10^{-6} m^2/s
A_1	Volumic rate of heat production in the upper crust (initially 20 km thick, Fig A2)	1.8 μW/m^3
A_2	Volumic rate of heat production in the lower crust (initially between 20 and 35 km deep in the crust, Fig A2)	0.75 μW/m^3

Figure captions

Fig 1. Diagram showing possible models for the growth of a continental plateau and its relationship to the adjacent transition zone. **a**) There is strong evidence for weak mid-/lower crust below plateaus and channel flows may also occur at depth. Less is known about the relationship between plateau and the transition zone. Three processes may occur in this zone adjacent to a neutral growing plateau: **b**) Channel Injection (CI); **c**) crustal thickening by accretion, in this case considered to be Viscous Thickening (VT); **d**) outward flow of unstable brittle upper and mid-crust, termed Plastic Translation (PT). Darker grey areas represent zones of high strain rate.

Fig 2. General Channel Injection(CI) model . Three crustal zones are considered: reference undeformed foreland crust; the transition zone (where crust thickens by accretion of injected material from/within the channel bounded by $S_1^{\pm}$); the plateau (characterized by nearly flat topography, $S_3 = S_{3p}$ = constant, and constant thickness crust, $H_c = H_{cp}$). Crust has uniform density ρ. The boundary condition is the flux of material from the plateau into the channel, q_b. Material flow in the transition zone channel comprises a Poiseuille flow driven by the transitional zone topographic gradient.

Fig 3. Results for Channel Injection model CI-1. Special case considered here includes: $\mu = 3 \times 10^{20}$ Pa·s, $h = 10$ km. Flux of material into the system, $q_b = 10^{-6}$ m^3/s per m along strike (average rate is 3.3 mm/y in 10 km channel), results in plateau margin elevated to 5.5 km in 20 My. Results are the same for constant h^3/μ (e.g. $\mu_{15} = 10^{21}$ Pa·s (for $h = 15$ km) or $\mu_{20} = 2.4 \times 10^{21}$ Pa·s (for $h = 20$ km). Note: (1) results do not depend on the vertical position of the channel within the crust; (2) model does not address connection with plateau.

Fig 4. Results for Channel Injection model CI-2. Special case considered here: thickness of the channel $h = 10$ km; $\mu = 10^{20}$ Pa·s if the depth of the centre of the channel, $d(x,t) < D^* = 50$ km, and $\mu = 10^{18}$ Pa·s otherwise. Flux of material into the system, $q_b = 4 \times 10^{-6}$ m^3/s per m along strike (average rate is 1.5 cm/y in 10 km channel) results in plateau margin elevated to 5.5 km in 20 My. Note: (1) decrease in viscosity under transitional crust leads to plateau type topography; (2) self-similar widening of the plateau is characterized by the plateau advancing velocity V_a and by kinematic-wave form of evolution of upper surface $S_3 = S_3(x + V_a t)$; (3) results are the same for constant h^3/μ; (4) channel flux varies spatially: under the plateau $q \approx q_b = const$, and in the transition zone flux decreases.

Fig 5. Comparison of the final geometry of Channel Injection model CI-1 (dash line, see details on Fig. 3) and transitional zone predicted by the Channel Injection model CI-2 designed to achieve the same geometry (solid line, see details on Fig. 4). Similar geometry is, however, obtained for different viscosities and flux into the system because the model CI-2 accounts the connection to plateau. See text for details.

Fig 6. Results for Channel Injection model CI-3. Special case considered here: $\mu = 10^{20}$ Pa·s if temperature in the channel is below critical $T < T^* = 750°$C, and $\mu = 4 \times 10^{18}$ Pa·s if $T > T^*$. Channel thickness is initially h_o. It then increases to include mid- and upper crust where $T > T^*$. Other parameters are the same as on Fig. 4. Note: (1) decrease in viscosity under transitional crust leads to plateau; (2) self-similar widening of the plateau is characterized by the plateau advancing velocity V_a and by kinematic-wave form of evolution of upper surface $S_3 = S_3(x + V_a t)$; (3) control parameter for the model is h^3/μ (demonstrated by the effective viscosity, dot line on **c**), but here h and μ are determined independently by the thermal state; (4) channel flux varies spatially: under the plateau $q \approx q_b = const$ and in the transition zone flux decreases.

Fig 7. Comparison of the final geometry of Channel Injection models CI-3 (dash line, see details on Fig. 6) and CI-2 (solid line, see details on Fig. 4). Similar geometry is obtained but for a different viscosity decrease under the plateau owing to thicker channel in the model CI-3. See text for details.

Fig 8. Comparison of the temperature rise after thickening the crust by 30 km at a constant rate for either the Channel Injection mode (solid line) and Pure Share mode of thickening (dash line). The thermal state depends on the time during which thickening occurs, but CI heats crust faster than PS. Note that although the initial distribution of radioactive heat sources are equal for two models, the PS model results in thicker highly radioactive crustal layer (up to 44 km at the edge of plateau) than CI-3 model (which thickens the upper, high-radioactivity crust up to 22 km). See details of the thermal model in Appendix. Dotted vertical line indicates the duration of thickening for the reference model.

Fig 9. (**a**–**b**) Contour plots of the final temperature in the middle of the transitional channel for Channel Injection (**a**) and Pure Shear (**b**) models. (**c**) Areas of thermal parameters of the crust (radioactivity of the upper crust, A_1 (initial thickness 20 km) and heat capacity, C_p) that can result in a consistency between thermal and mechanical models (grey). The other parameters are the same as in the reference model (Table 1). The circles illustrate thermal parameters of the reference model (RM), and ones used to model Tibet (Beaumont *et al.* 2004) and Andes Altiplano (Babeyko *et al.* 2002).

Fig 10. Dependence of effective viscosity of quartzite on temperature and strain rate. Here we approximate thermal and strain regime inside the channel in the transitional zone. The foreland end of the channel is characterized by low temperature (300–400°C) and low strain rate ($\leq 10^{15}$ s^{-1}). The plateau end of the transitional channel has high temperature (700–800°C) and high strain rate (up to 2×10^{13} s^{-1} for the reference model). The plot shows variations of effective viscosity of more than two orders of magnitude over the evolution of the transitional channel. Laboratory data based on the compilation of Gleason & Tullis (1995, Table 3).

Fig 11. Dependence of topography of the transitional zone on the variations of viscosity along the transitional channel. The result of CI-3 (constant viscosity along the channel, solid line) differs significantly from the model with exponential decrease of channel viscosity during evolution of the transition zone (dash line). The latter model (see text) is based on the experimental results presented on Fig. 10.

Fig 12. Results for Viscous Thickening model. Special case considered here has $\mu = 1.5 \times 10^{22}$ Pa·s. Flux of material into the system, $q_b = 10^{-6}$ m^3/s per m along strike (as for Fig. 3) results in plateau margin elevated to 5.5 km in 20 My. The geometry of the transitional zone is similar to one by CI-3 (Fig. 7), but rheological parameters of these two models differ significantly.

Fig 13. Geometry and forces for simplified analysis of the stability of brittle upper crust of the transition zone (block with bold outline). The brittle block is underlain by a mid-crustal channel and material accreted from the channel. Only forces that contribute to the horizontal balance are indicated.

Fig A1. Thermal evolution of the Pure Shear model. (**a**) Evolution of temperature at the base of the middle crust (5 km above the lower crust, dotted line in **b**). (**b**) General view on the evolution of a vertical Lagrangian crustal column. Dark grey indicates upper and middle crust that thickens uniformly, light grey is lower, undeformable crust. The dash-dot line separates crust into highly radioactive ($A = A_1$) and low-radioactive ($A = A_1$) parts. The underlying mantle lithosphere (the depth of the model is 90-100 km) has zero radioactivity. The isotherms ($T^* = 750°$C, solid line, and $T = 700°$C, dash line) indicate compatibility of the thermal and mechanical models (see Sections 1.3 and 2.1).

Fig A2. Thermal evolution of the Channel Injection (CI) model: (**a**) Evolution of the mid-channel temperature, and (**b**) general view on the thermal and thickening evolution of a vertical Lagrangian crustal column. Levels of grey (from lighter to darker) indicate: upper and low undeformable crust; material accreted from the channel; the high-viscosity channel in the transition crust; low-viscosity channel beneath the plateau. See details of design in Fig A1. Note that the highly radioactive portion of the crust thickens much less than in the pure shear model.

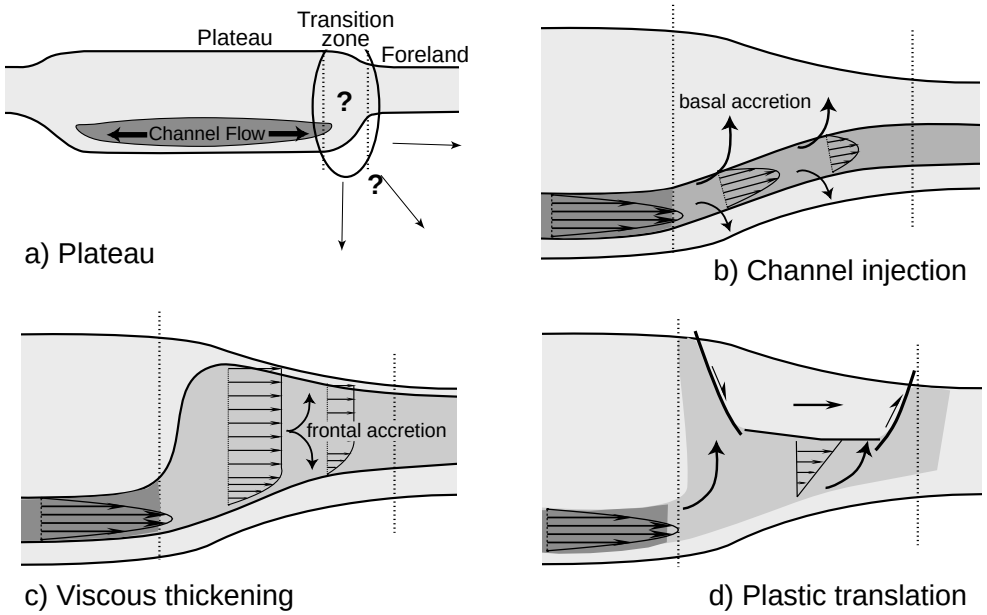

Fig 1. Diagram showing possible models for the growth of a continental plateau and its relationship to the adjacent transition zone. **a**) There is strong evidence for weak mid-/lower crust below plateaus and channel flows may also occur at depth. Less is known about the relationship between plateau and the transition zone. Three processes may occur in this zone adjacent to a neutral growing plateau: **b**) Channel Injection (CI); **c**) crustal thickening by accretion, in this case considered to be Viscous Thickening (VT); **d**) outward flow of unstable brittle upper and mid-crust, termed Plastic Translation (PT). Darker grey areas represent zones of high strain rate.

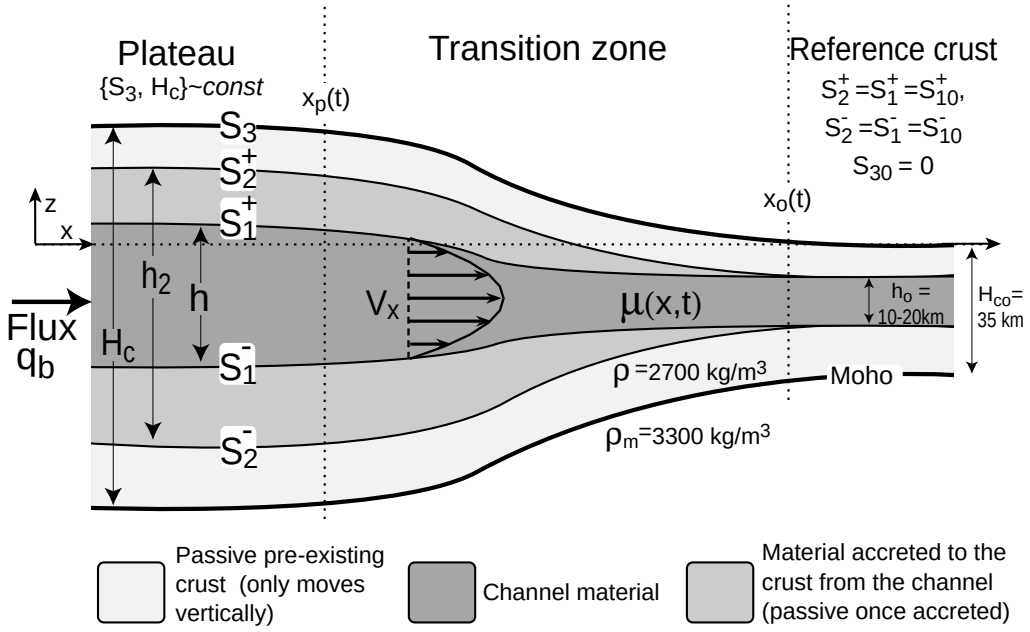

Fig 2. General Channel Injection(CI) model . Three crustal zones are considered: reference undeformed foreland crust; the transition zone (where crust thickens by accretion of injected material from/within the channel bounded by $S_1^{\pm}$); the plateau (characterized by nearly flat topography, $S_3 = S_{3p}$ = constant, and constant thickness crust, $H_c = H_{cp}$). Crust has uniform density ρ. The boundary condition is the flux of material from the plateau into the channel, q_b. Material flow in the transition zone channel comprises a Poiseuille flow driven by the transitional zone topographic gradient.

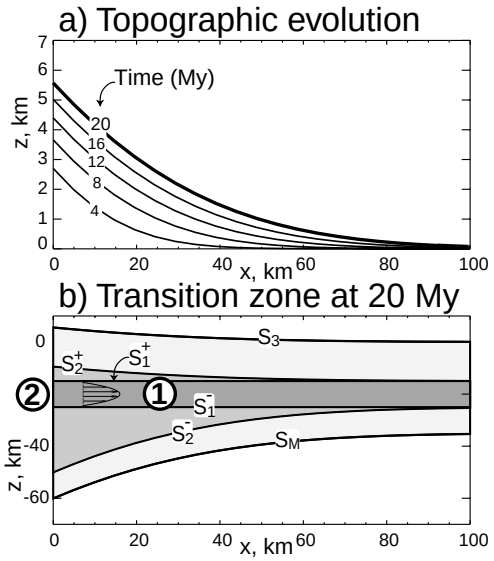

Fig 3. Results for Channel Injection model CI-1. Special case considered here includes: $\mu = 3 \times 10^{20}$ Pa·s, $h = 10$ km. Flux of material into the system, $q_b = 10^{-6}$ m^3/s per m along strike (average rate is 3.3 mm/y in 10 km channel), results in plateau margin elevated to 5.5 km in 20 My. Results are the same for constant h^3/μ (e.g. $\mu_{15} = 10^{21}$ Pa·s (for $h = 15$ km) or $\mu_{20} = 2.4 \times 10^{21}$ Pa·s (for $h = 20$ km). Note: (1) results do not depend on the vertical position of the channel within the crust; (2) model does not address connection with plateau.

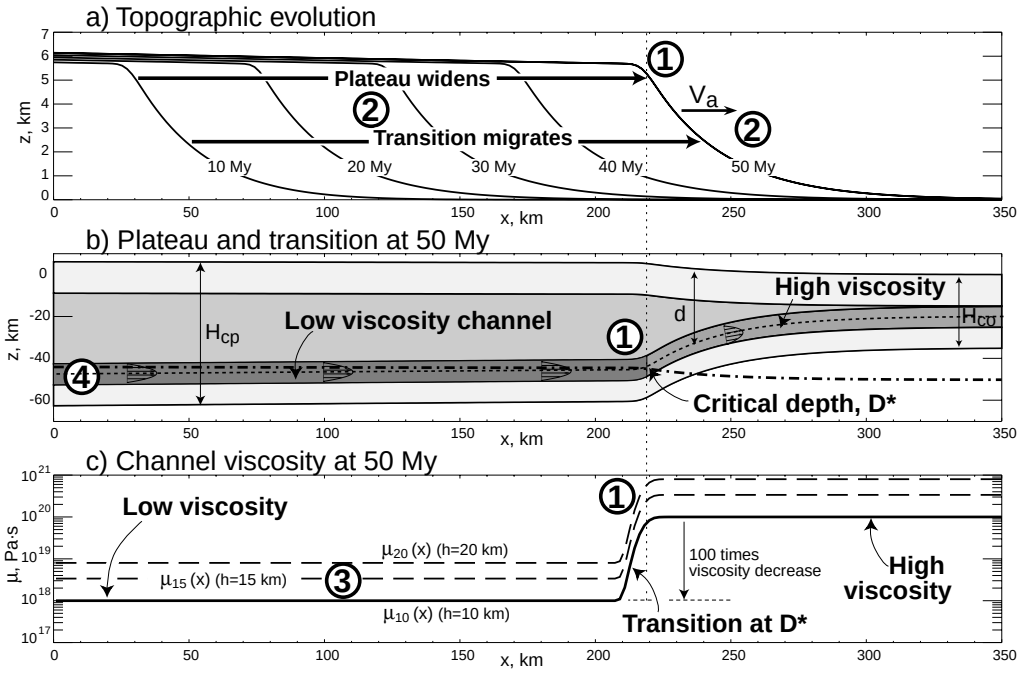

Fig 4. Results for Channel Injection model CI-2. Special case considered here: thickness of the channel $h = 10$ km; $\mu = 10^{20}$ Pa·s if the depth of the centre of the channel, $d(x,t) < D^* = 50$ km, and $\mu = 10^{18}$ Pa·s otherwise. Flux of material into the system, $q_b = 4 \times 10^{-6}$ m^3/s per m along strike (average rate is 1.5 cm/y in 10 km channel) results in plateau margin elevated to 5.5 km in 20 My. Note: (1) decrease in viscosity under transitional crust leads to plateau type topography; (2) self-similar widening of the plateau is characterized by the plateau advancing velocity V_a and by kinematic-wave form of evolution of upper surface $S_3 = S_3(x + V_a t)$; (3) results are the same for constant h^3/μ; (4) channel flux varies spatially: under the plateau $q \approx q_b = const$, and in the transition zone flux decreases.

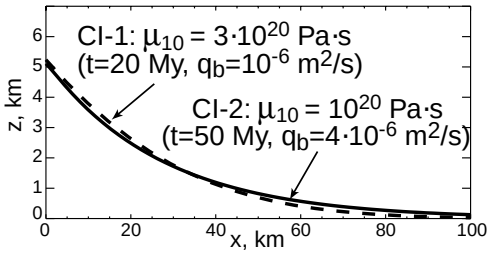

Fig 5. Comparison of the final geometry of Channel Injection model CI-1 (dash line, see details on Fig. 3) and transitional zone predicted by the Channel Injection model CI-2 designed to achieve the same geometry (solid line, see details on Fig. 4). Similar geometry is, however, obtained for different viscosities and flux into the system because the model CI-2 accounts the connection to plateau. See text for details.

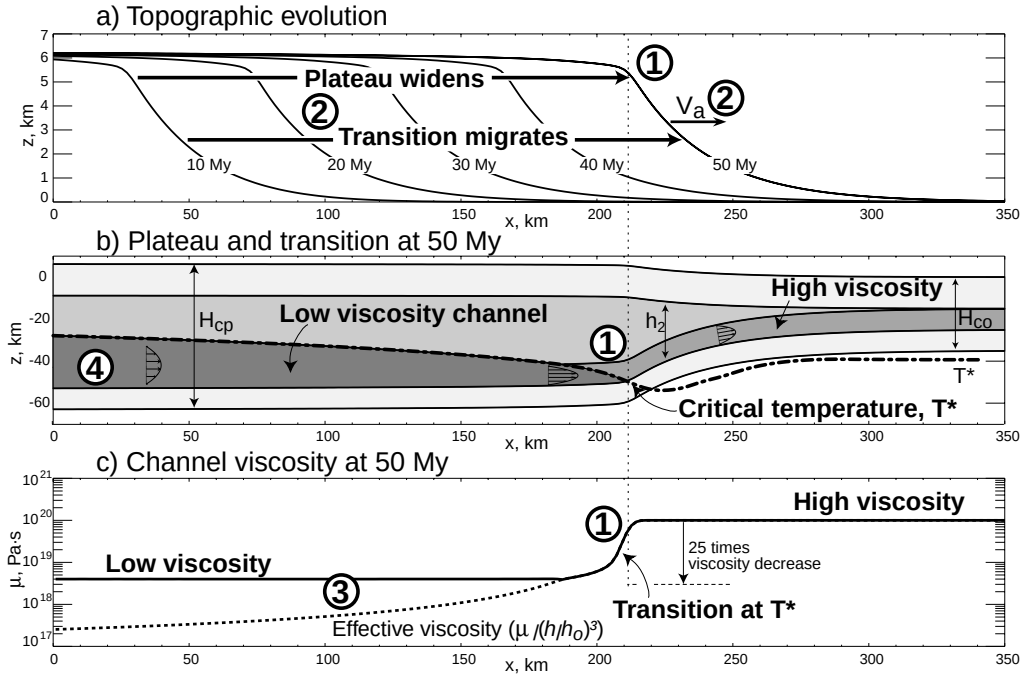

Fig 6. Results for Channel Injection model CI-3. Special case considered here: $\mu = 10^{20}$ Pa·s if temperature in the channel is below critical $T < T^* = 750°$C, and $\mu = 4 \times 10^{18}$ Pa·s if $T > T^*$. Channel thickness is initially h_o. It then increases to include mid- and upper crust where $T > T^*$. Other parameters are the same as on Fig. 4. Note: (1) decrease in viscosity under transitional crust leads to plateau; (2) self-similar widening of the plateau is characterized by the plateau advancing velocity V_a and by kinematic-wave form of evolution of upper surface $S_3 = S_3(x + V_a t)$; (3) control parameter for the model is h^3/μ (demonstrated by the effective viscosity, dot line on **c**), but here h and μ are determined independently by the thermal state; (4) channel flux varies spatially: under the plateau $q \approx q_b = const$ and in the transition zone flux decreases.

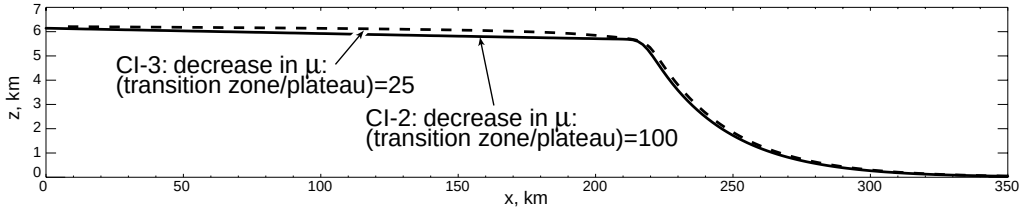

Fig 7. Comparison of the final geometry of Channel Injection models CI-3 (dash line, see details on Fig. 6) and CI-2 (solid line, see details on Fig. 4). Similar geometry is obtained but for a different viscosity decrease under the plateau owing to thicker channel in the model CI-3. See text for details.

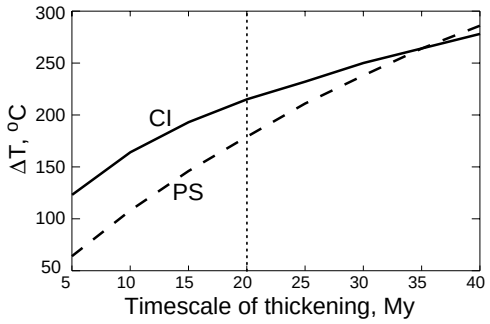

Fig 8. Comparison of the temperature rise after thickening the crust by 30 km at a constant rate for either the Channel Injection mode (solid line) and Pure Share mode of thickening (dash line). The thermal state depends on the time during which thickening occurs, but CI heats crust faster than PS. Note that although the initial distribution of radioactive heat sources are equal for two models, the PS model results in thicker highly radioactive crustal layer (up to 44 km at the edge of plateau) than CI-3 model (which thickens the upper, high-radioactivity crust up to 22 km). See details of the thermal model in Appendix. Dotted vertical line indicates the duration of thickening for the reference model.

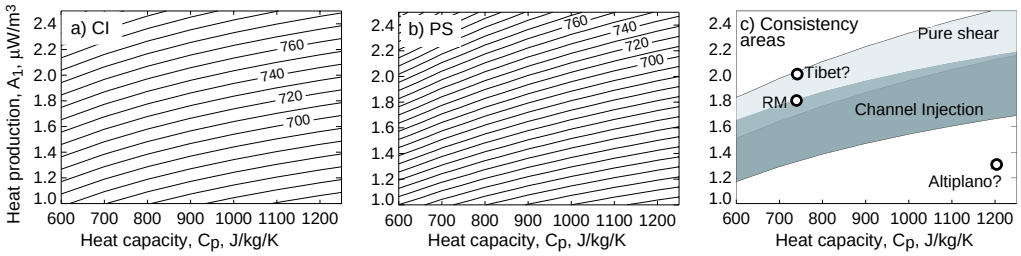

Fig 9. (**a**–**b**) Contour plots of the final temperature in the middle of the transitional channel for Channel Injection (**a**) and Pure Shear (**b**) models. (**c**) Areas of thermal parameters of the crust (radioactivity of the upper crust, A_1 (initial thickness 20 km) and heat capacity, C_p) that can result in a consistency between thermal and mechanical models (grey). The other parameters are the same as in the reference model (Table 1). The circles illustrate thermal parameters of the reference model (RM), and ones used to model Tibet (Beaumont *et al.* 2004) and Andes Altiplano (Babeyko *et al.* 2002).

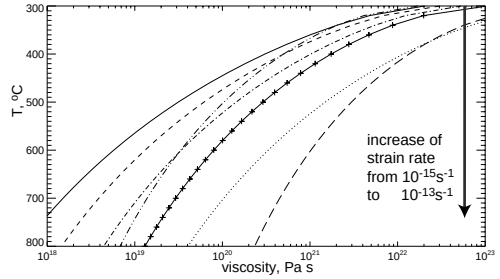

Fig 10. Dependence of effective viscosity of quartzite on temperature and strain rate. Here we approximate thermal and strain regime inside the channel in the transitional zone. The foreland end of the channel is characterized by low temperature (300–400°C) and low strain rate ($\leq 10^{15}$ s^{-1}). The plateau end of the transitional channel has high temperature (700–800°C) and high strain rate (up to 2×10^{13} s^{-1} for the reference model). The plot shows variations of effective viscosity of more than two orders of magnitude over the evolution of the transitional channel. Laboratory data based on the compilation of Gleason & Tullis (1995, Table 3).

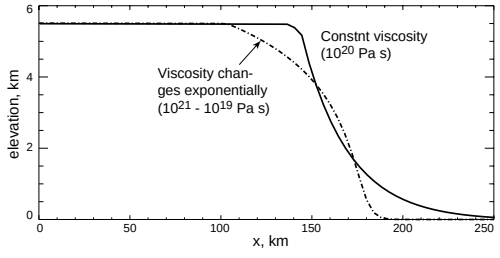

Fig 11. Dependence of topography of the transitional zone on the variations of viscosity along the transitional channel. The result of CI-3 (constant viscosity along the channel, solid line) differs significantly from the model with exponential decrease of channel viscosity during evolution of the transition zone (dash line). The latter model (see text) is based on the experimental results presented on Fig. 10.

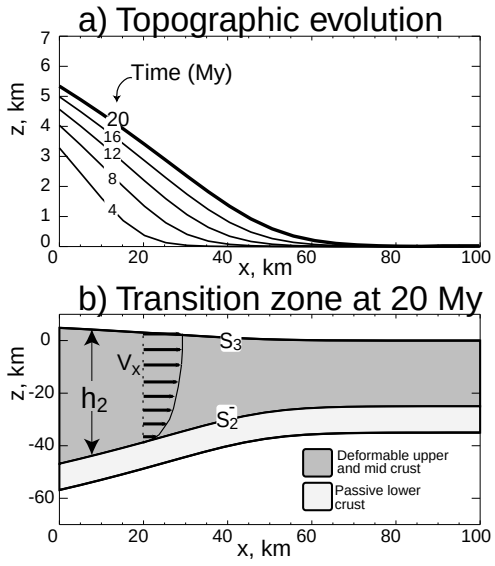

Fig 12. Results for Viscous Thickening model. Special case considered here has $\mu = 1.5 \times 10^{22}$ Pa·s. Flux of material into the system, $q_b = 10^{-6}$ m^3/s per m along strike (as for Fig. 3) results in plateau margin elevated to 5.5 km in 20 My. The geometry of the transitional zone is similar to one by CI-3 (Fig. 7), but rheological parameters of these two models differ significantly.

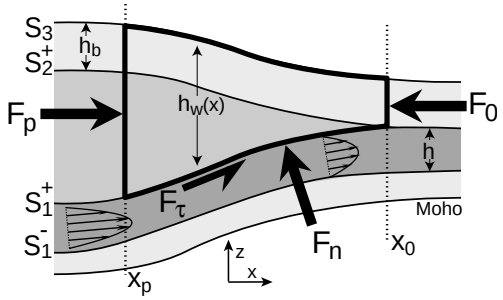

Fig 13. Geometry and forces for simplified analysis of the stability of brittle upper crust of the transition zone (block with bold outline). The brittle block is underlain by a mid-crustal channel and material accreted from the channel. Only forces that contribute to the horizontal balance are indicated.

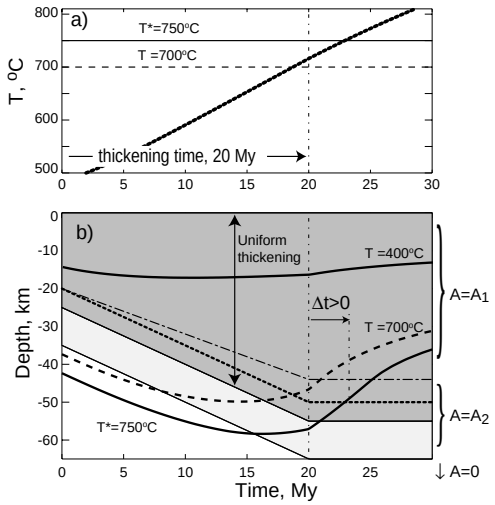

Fig A1. Thermal evolution of the Pure Shear model. (**a**) Evolution of temperature at the base of the middle crust (5 km above the lower crust, dotted line in **b**). (**b**) General view on the evolution of a vertical Lagrangian crustal column. Dark grey indicates upper and middle crust that thickens uniformly, light grey is lower, undeformable crust. The dash-dot line separates crust into highly radioactive ($A = A_1$) and low-radioactive ($A = A_1$) parts. The underlying mantle lithosphere (the depth of the model is 90-100 km) has zero radioactivity. The isotherms ($T^* = 750°$C, solid line, and $T = 700°$C, dash line) indicate compatibility of the thermal and mechanical models (see Sections 1.3 and 2.1).

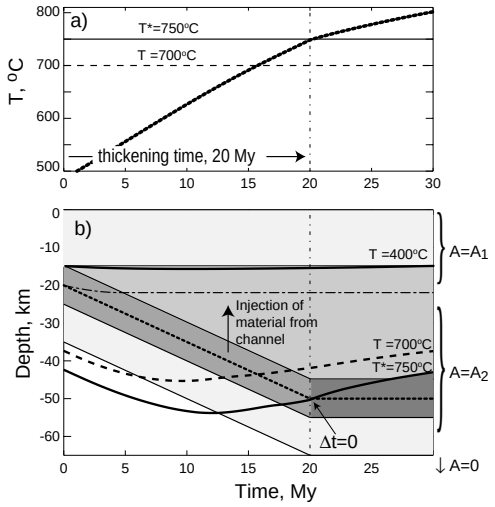

Fig A2. Thermal evolution of the Channel Injection (CI) model: (**a**) Evolution of the mid-channel temperature, and (**b**) general view on the thermal and thickening evolution of a vertical Lagrangian crustal column. Levels of grey (from lighter to darker) indicate: upper and low undeformable crust; material accreted from the channel; the high-viscosity channel in the transition crust; low-viscosity channel beneath the plateau. See details of design in Fig A1. Note that the highly radioactive portion of the crust thickens much less than in the pure shear model.